APL Photonics

Surface profile-tailored magneto-optics in magnetoplasmonic crystals

Cite as: APL Photonics **7**, 026104 (2022); https://doi.org/10.1063/5.0072698
Submitted: 24 September 2021 • Accepted: 18 January 2022 • Accepted Manuscript Online: 20 January 2022 • Published Online: 03 February 2022

Maxim A. Kiryanov, Aleksandr Yu. Frolov, Ilya A. Novikov, et al.

Surface profile-tailored magneto-optics in magnetoplasmonic crystals

Cite as: APL Photon. 7, 026104 (2022); doi: 10.1063/5.0072698
Submitted: 24 September 2021 • Accepted: 18 January 2022 •
Published Online: 3 February 2022

Maxim A. Kiryanov, Aleksandr Yu. Frolov, Ilya A. Novikov, Polina A. Kipp, Polina K. Nurgalieva, Vladimir V. Popov, Aleksandr A. Ezhov, Tatyana V. Dolgova, and Andrey A. Fedyanin[a)]

AFFILIATIONS

Faculty of Physics, Lomonosov Moscow State University, 119991 Moscow, Russia

[a)]Author to whom correspondence should be addressed: fedyanin@nanolab.phys.msu.ru

ABSTRACT

The control of transverse magneto-optical Kerr effect (TMOKE) enhancement is realized by balancing the radiative and absorption losses in one-dimensional all-nickel magnetoplasmonic crystals. The modulation of the surface shape tunes the plasmonic radiative losses and coupling of the incident light with surface plasmons. The maximal magneto-optical response corresponds to the optimal coupling implemented with the equality of radiative and absorption losses. A slight deviation from the optimal corrugation depth results in a significant reduction of the TMOKE value.

I. INTRODUCTION

The past decade of plasmonics has witnessed numerous approaches to fine-tune the optical resonances for biomedical applications,[1–3] photovoltaics,[4] and sensing.[5,6] The shape and size as well as the dielectric environment of plasmonic nanoparticles and surfaces are viable instruments for tailoring resonance spectral positions and line shapes. Plasmonic nanosystems of various types, such as gold and silver nanospheres, composite nanoshells,[1,7] nanorods,[1,8] perforated, and modulated surfaces have been studied both theoretically and experimentally. Surface-enhanced Raman scattering[9] and enhanced nonlinear optics[10] as well as plasmon rulers,[11] metalenses, metasurfaces,[12,13] and waveguides[14,15] have been demonstrated. In addition, the concept of active plasmonics[16,17] allows post-fabrication tuning of plasmonic resonances by external impacts, such as temperature,[18,19] electric[20,21] and magnetic[22,23] field applications, and laser pumps[24,25] as well as their combination.[26] Apart from harnessing active plasmonics with magnetic fields for various potential applications, the nanoplasmonics of magnetic media is a growing fundamental research area due to salient magneto-optical effects.[27,28] The combination of high optical field concentration and magneto-optical activity yields a resonant enhancement of Kerr[29,30] and Faraday[31] effects. Surface plasmon (SP) excitation in specially designed nanostructured materials provides light localization, while magnetic field application affects the wave vector of propagating surface plasmon making a magnetoplasmonic device active.[23]

Despite high absorption losses in ferromagnetic metals, these metals are widely used as a basis for plasmonic systems and potential devices.[32–41] Considerable effort was made to optimize the optical losses and to improve the maximal magneto-optical figure-of-merit. The examples are composite magnetoplasmonic systems which consist of a nanostructured noble-metal film on top of a magnetic dielectric,[42,43] multilayer noble/ferromagnetic metal thin films,[29,44,45] magnetoplasmonic crystals (MPCs),[46,47] and noble-metal nanoparticles in a magnetic dielectric matrix.[48,49]

Another approach to improve the SP-assisted magneto-optical effects is the structural-design control of radiative SP losses associated with scattering of SPs to far-field. A two-dimensional arrangement of individual ferromagnetic nanoparticles allows suppression of the radiative losses by the excitation of surface lattice modes.[50,51] The adjustment of a stripe width and ferromagnetic layer thickness in MPCs provides the improvement of the SP quality factor, which enhances the polar, longitudinal, and transverse magneto-optical Kerr effect (TMOKE).[52–54] Subradiant dark plasmonic modes provide stronger magneto-optical enhancement in MPCs[47] and nanocavities[55] in comparison with bright dipole active modes. Radiative losses can also be significantly suppressed by hybridization of broad localized plasmons with a narrow

waveguide mode. It results in the electromagnetically induced absorption effect and giant Faraday rotation.[56] The idea of losses balanced by corrugation depth tuning appeared to be fruitful for control of reflectance spectra[57,58] and optimal light-to-plasmon coupling[59] in one-dimensional plasmonic crystals. This approach can be applied to the optimization of the MPC magneto-optical response.

In this paper, the SP-assisted TMOKE enhancement is controlled by the variation in the corrugation depth h providing the balance of the radiative (Γ_{rad}) and absorption (Γ_{abs}) losses in 1D all-nickel MPCs. The influence of the MPC corrugation depth on the SP radiative losses allows us to achieve the optimal coupling condition and strongest TMOKE enhancement. Numerical simulations and experiment demonstrate that appropriate adjustment of the corrugation depth provides the maximal TMOKE and magneto-optical figure-of-merit (FOM). The reflectance spectrum of the optimal sample reveals zero dip, which is known to correspond to the optimal light-to-SP coupling condition ($\Gamma_{abs} = \Gamma_{rad}$).[59] The TMOKE values of 2.3% are achieved in the experiment. Any deviation from the optimal depth suppresses TMOKE.

II. EXPERIMENTAL RESULTS

A set of three one-dimensional all-nickel MPCs with the shape of the surface close to sinusoidal, the same spatial period, and different corrugation depths h (inset in Fig. 1) was studied. To characterize the spatial profile of each sample, we carried out atomic force microscopy (AFM) and scanning electron microscopy (SEM) measurements (top panels in Fig. 1). The obtained values of the surface corrugation depth were 90 ± 5, 125 ± 5, and 165 ±5 nm for Samples 1, 2, and 3, respectively. Optical diffraction measurements revealed that the spatial period of all samples was equal to 503 ± 2 nm. More details on sample fabrication and characterization can be found in Sec. I of the supplementary material.

The reflectance spectra of the studied samples were measured for the incident angles θ within the range of 5°–45° (Fig. 1, bottom panels). All spectra possess an asymmetric Fano-type resonance, comprising a sharp peak followed by a dip. The peak corresponds to the Rayleigh anomaly related to the fading diffraction order that propagates along the sample surface, while the dip refers to the Wood anomaly associated with SP excitation.[60] The red spectral shift of the SP resonance with the incident angle increase provides the evidence of the SP excitation by the 1st diffraction order.

Figure 1 shows that the reflectance spectra of MPCs are strongly profile-dependent. The increase in h results in the SP resonance broadening and growth of the reflectance at the SP dip (R_{dip}). Such behavior of the resonance is governed by the balance of SP radiative and absorption losses (see Sec. III). The most profound SP resonance coupled with an almost zero reflectance is observed for the MPC with the lowest corrugation depth (Sample 1). Lowering of the non-resonant plateau to the left of the Rayleigh anomaly with an increase in h is attributed to the redistribution of light energy between 0th and 1st diffraction orders.[61]

The studied set of MPCs also supports another type of excitation that emerges in Sample 3 around λ = 550 nm. The corresponding resonance is spectrally broad, has no dependence on the angle of incident light, and is revealed in samples with high surface corrugation values (Sample 3 reflectance spectrum in Fig. 1). This allows identifying the excitation as the standing-wave surface plasmon (SWSP),[62,63] which is a standing analog of SP emerging on the walls of the grating grooves. The SWSP resonance can be spectrally shifted through the change in the corrugation depth in contrast to the SP resonance shifting through the variation in the light incidence angle. More details on the SWSP can be found in Sec. II of the supplementary material.

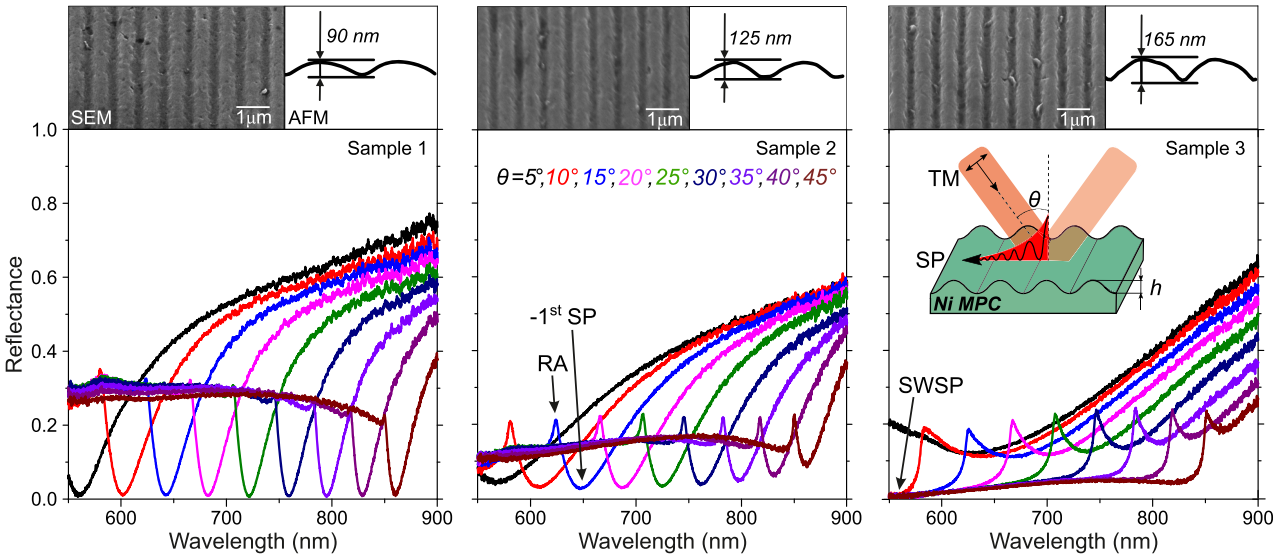

FIG. 1. Top panels: SEM images and AFM cross sections. Bottom panels: the MPC specular reflectance spectra for a set of incident angles. p-polarized light is used. The inset illustrates the experimental scheme.

Magneto-optical measurements were carried out in the TMOKE configuration by the lock-in detection technique in an alternating magnetic field with an amplitude of H = 500 Oe. The value of TMOKE was determined as follows:

$$\delta = \frac{R(+H) - R(-H)}{R(0)}, \quad (1)$$

where $R(\pm H)$ and $R(0)$ are reflectances with and without the external magnetic field, respectively. The contribution of the remanent magnetization to reflectance is below 2% and neglected. Figure 2 shows the experimental spectra of reflectance (black circles) and TMOKE (blue circles) measured at the incident angle of 25°. The SP-induced TMOKE enhancement as well as spectra modification are observed for all samples in comparison with the bulk nickel (Fig. 2, open circles). Each TMOKE spectrum has a resonant feature comprising the peak and the dip with sign change. The SP-resonant TMOKE peak in Sample 3 is modified by overlapping with the SWSP resonance.

The TMOKE enhancement value and the line shape are strongly profile-dependent. The corrugation depth increase results in the suppression and broadening of the SP-resonant TMOKE. Moreover, its spectrum becomes more asymmetrical. TMOKE reaches 2.3%, −0.8%, and −0.5% in the vicinity of the SP resonance for Samples 1, 2, and 3, respectively. The SP excitation provides 75× (Sample 1), 27× (Sample 2), and 23× (Sample 3) TMOKE enhancement in comparison with the non-structured nickel plate. The magneto-optical figure-of-merit (FOM), defined as $\delta(\%) \cdot R(0)$, reaches the highest value in Sample 1 (0.1%), while the corresponding values for Samples 2 and 3 (0.06% for both) and the reference plate (0.015% at 725 nm) are lower (see the magneto-optical FOM spectra in Fig. S2 of the supplementary material). Therefore, a high TMOKE value in Sample 1 is attributed to the significant FOM rather than to the division by a low reflectance at the SP resonance [see Eq. (1)]. The FOM maxima are shifted relative to the TMOKE extrema by several nanometers.

The TMOKE enhancement in MPCs is mainly attributed to the magnetic-field-induced shift of the SP-resonant wavelength.[64] The shift is determined by dielectric functions of the metal and a surrounding dielectric as well as gyration. Since all the studied samples are made of the same material and the same magnetic field is applied, the induced shift is almost equal for each sample. Therefore, the enhancement values depend on the properties of the SP resonance and will be discussed below.

Broadband enhancement of the TMOKE in Sample 3 spectrum is observed in the vicinity of 550 nm at the SWSP resonance. The maximal values achieved are even higher than those in the SP-resonant spectral area. Since the maximal FOM of the SWSP-induced TMOKE, 0.015% at 600 nm, is twice as low as that in the reference plate at the same wavelength, high TMOKE values are attributed to the low reflectance in the resonant region. The latter is due to the incident light diffracting into the 1st order rather than into the 0th order. The rapid growth of reflectance at the Rayleigh anomaly at 715 nm triggers the drop of TMOKE. In turn, SP starts to contribute to the effect. Two resonances merge and the inflection point appears in the TMOKE spectrum.

III. SIMULATIONS AND DISCUSSION

The width of the SP resonance is attributed to SP losses: $\Gamma = \Gamma_{rad} + \Gamma_{abs}$.[6] Absorption losses Γ_{abs} are mostly defined by the material dispersion and slightly depend on the corrugation depth. On the contrary, radiative losses Γ_{rad} depend on the surface profile and get higher with an increase in h.[65] Therefore, the SP resonance is broader for a more corrugated surface. It is known that the equality of radiative and absorption losses, $\Gamma_{rad} = \Gamma_{abs}$, leads to a destructive Fano interference of non-resonant and SP-re-emitted light with zero reflectance.[57,66] The latter also corresponds to the case of optimal coupling of the light with the SP mode in various plasmonic systems.[59,67–69] Since radiative losses are profile-dependent, the optimal coupling and zero reflectance are achieved by corrugation depth tailoring. To determine the optimal depth, MPC reflectance spectra were calculated via the finite-difference time-domain (FDTD) method. The surface profiles of the studied MPCs as well as the experimental configuration (p-polarized light and the same set of angles of incidence) were reproduced in the numerical modeling.

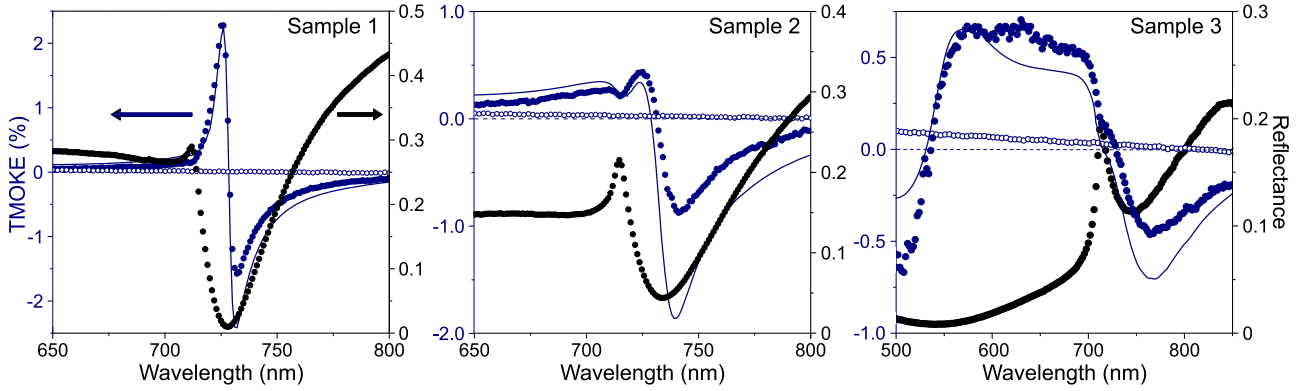

FIG. 2. Experimental (solid blue circles) and simulated (solid blue curves) TMOKE spectra for the set of studied samples. The open blue circles show the experimental TMOKE spectra of the non-structured Ni surface. The experimental reflectance of MPCs is shown by solid black circles. The angle of incidence is 25°. The incident light is p-polarized.

The amplitudes of spatial harmonics were fitting parameters varied around the AFM data (see Sec. I of the supplementary material). The simulated reflectance spectra shown in Fig. 3 express the features similar to those observed in the experiment, particularly the reflectance value at the SP dip (R_{dip}) is close to zero for Sample 1 (red circle marks in Fig. 3). Then, the spatial period and the surface shape of the grating were fixed to numerically study the set of MPCs with various corrugation depths (the right inset in Fig. 3). The latter significantly affects the line shape of MPC spectra. The dependence of R_{dip} on h is non-monotonic, and three cases can be distinguished: the descending one for $h < 90$ nm, close to zero reflectance at $h \approx 90$ nm, and the ascending one in the case of $h > 90$ nm.

Therefore, the optimal coupling is achieved at $h \approx 90$ nm, while $h < 90$ nm and $h > 90$ nm are the cases of under-coupling and over-coupling regimes, respectively. MPCs used in the experiment correspond to the optimal coupling (Sample 1), over-coupling (Sample 2), and strong over-coupling (Sample 3). Optimal coupling provides not only the most profound SP resonance in reflectance but also the strongest electromagnetic field localization (see the top panels in Fig. 3). Field localization defines the interaction between the light and matter and, consequently, directly affects the magneto-optical effect value.[30] That is why the strongest TMOKE enhancement is inherent to Sample 1 with the corrugation depth close to the optimal one. However, the considered samples do not support the under-coupling regime. We studied another set of MPCs where all three coupling regimes were realized (see Sec. IV of the supplementary material). The sample with the optimal coupling demonstrates higher TMOKE values relative to those with under- and over-coupling.

The TMOKE in non-sinusoidal MPCs is lower due to higher losses and weaker electromagnetic field localization (see Sec. V of the supplementary material). The observed TMOKE values in Sample 1 are an order of magnitude higher than those reported earlier for rectangular all-nickel MPCs[32,34] with a weak coupling between the light and the SP mode ($\Gamma_{abs} \neq \Gamma_{rad}$). It means that the MPC surface shape optimization is another way of magneto-optical response improvement.

The TMOKE spectra (blue solid curves in Fig. 2) of the studied MPCs were simulated by the FDTD method in the Comsol Multiphysics package. The spectral dependences of the Ni dielectric permittivity and gyration were taken from Refs. 70 and 71, respectively. The simulations qualitatively reproduce the experimental dependences of TMOKE on h. The discrepancy in the absolute values of the TMOKE is due to the surface shape and material properties mismatch for real and modeled structures, light beam divergence, etc.

However, a conventional measure of magneto-optical efficiency is the magneto-optical FOM since the TMOKE can infinitely grow with reflectance tending to zero. To find the optimal design and show the influence of the light-to-SP coupling on the magneto-optical response, the FOM was numerically modeled for a series of corrugation depths (Fig. 4). The magneto-optical FOM value maximal over the studied spectral range (blue curve) is shown along with reflectance (red curve) at the corresponding wavelength. R_{dip} (black curve) illustrates the light-to-SP coupling efficiency. The highest FOM value of 0.18% is achieved at the corrugation depth of optimal light-to-SP coupling ($h = 97$ nm, R_{dip} minimum). The experimentally observed maximal FOM of 0.1% at $h = 90$ nm (close to the simulated optimum) is higher than that in hybrid noble metal–dielectric systems[72] (FOM = 0.085%) and comparable with all-dielectric magnetic metasurfaces[73] (FOM = 0.15%) and nickel-based Mie-resonant hybrid systems[36] (FOM = 0.2%). Despite common misconception, Ni-based nanostructures demonstrate high performance among the variety of magnetophotonic systems.

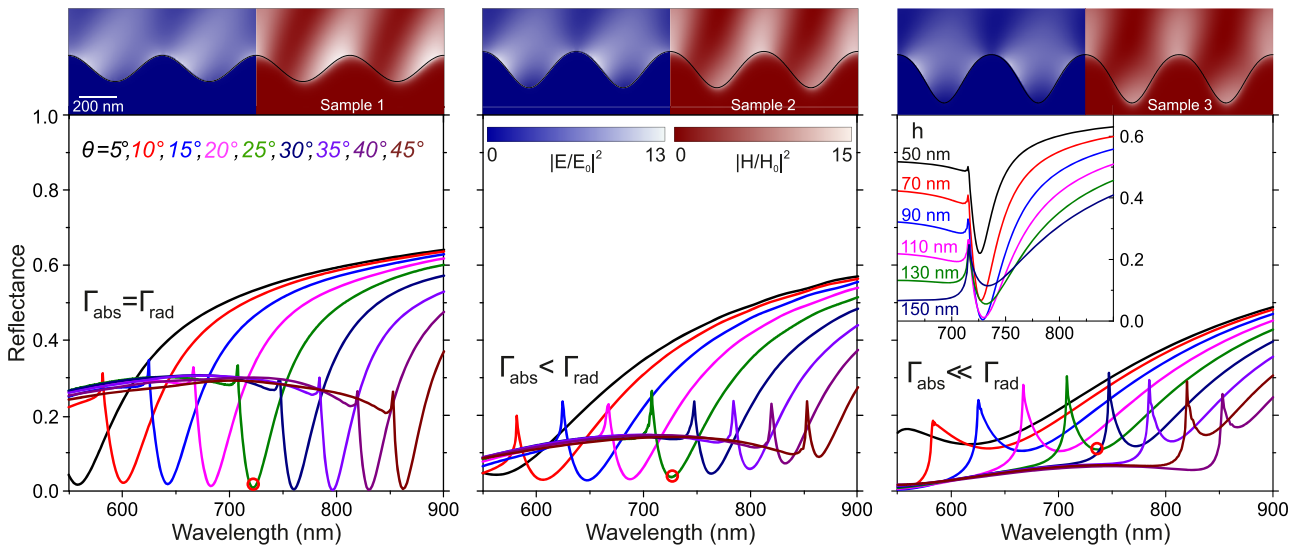

FIG. 3. Top panels: electromagnetic field distribution at the wavelength of the SP reflectance dip (indicated by open red circles). Bottom panels: simulated reflectance spectra of MPCs for the set of incident angles used in the experiment. (Inset) The dependence of the reflectance spectrum on the surface corrugation depth for $\theta = 25°$.

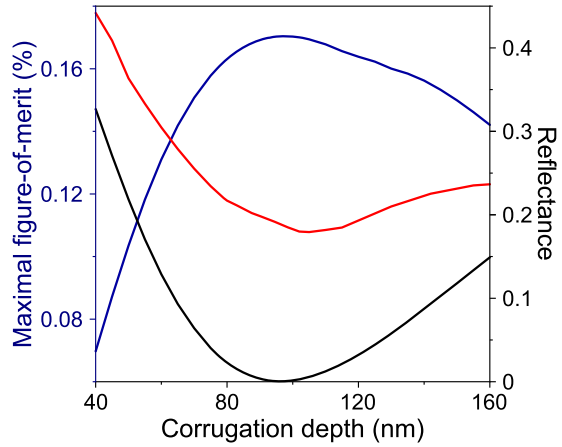

FIG. 4. Maximal values of the magneto-optical FOM over the studied spectral range (blue curve) along with reflectance (red curve) at the corresponding wavelength as a function of the corrugation depth. Black curve is the R_{dip} value for each corrugation depth.

IV. CONCLUSIONS

We have demonstrated experimentally and numerically that appropriate adjustment of the corrugation depth provides the maximal TMOKE and magneto-optical FOM. The reflectance spectrum of the optimal sample reveals zero dip, which is known to correspond to the optimal light-to-SP coupling condition ($\Gamma_{abs} = \Gamma_{rad}$).[59] The recipe to achieve the equality is to tune SP radiative losses by changing the MPC corrugation depth. TMOKE and FOM values reach 2.3% and 0.1%, respectively, for the optimal configuration of the MPC surface. The TMOKE values are three times higher than the values for other corrugation depths as well as an order of magnitude higher than those reported earlier for all-nickel MPCs.[32,34] The suggested approach can improve SP-assisted magneto-optical effects in other configurations as well (longitudinal, polar Kerr, and Faraday) and expand the functionality of plasmonic-based magneto-optical devices.

SUPPLEMENTARY MATERIAL

See the supplementary material for details on the magnetoplasmonic crystal fabrication, standing wave surface plasmons, magneto-optical figure-of-merit of the experimental samples, and influence of the MPC surface shape on SP absorption losses.

ACKNOWLEDGMENTS

This research was supported by the Russian Foundation for Basic Research (Grant No. 20-02-00758, experiment) and the Russian Science Foundation (Grant No. 18-12-00475, calculations). This research was performed according to the Development Program of the Interdisciplinary Scientific and Educational School of Lomonosov Moscow State University "Photonic and Quantum technologies. Digital medicine." This study was partly supported by the MSU Quantum Technology Center.

AUTHOR DECLARATIONS

Conflict of Interest

The authors declare no conflicts of interest.

DATA AVAILABILITY

The data that support the findings of this study are available from the corresponding author upon reasonable request.

REFERENCES

[1]P. K. Jain, X. Huang, I. H. El-Sayed, and M. A. El-Sayed, "Noble metals on the nanoscale: Optical and photothermal properties and some applications in imaging, sensing, biology, and medicine," Acc. Chem. Res. **41**, 1578 (2008).
[2]K. A. Willets and R. P. Van Duyne, "Localized surface plasmon resonance spectroscopy and sensing," Annu. Rev. Phys. Chem. **58**, 267 (2007).
[3]J. Jiang, X. Wang, S. Li, F. Ding, N. Li, S. Meng, R. Li, J. Qi, Q. Liu, and G. L. Liu, "Plasmonic nano-arrays for ultrasensitive bio-sensing," Nanophotonics **7**, 1517 (2018).
[4]H. A. Atwater and A. Polman, "Plasmonics for improved photovoltaic devices," Nat. Mater. **9**, 205 (2010).
[5]M. I. Stockman, "Nanoplasmonic sensing and detection," Science **348**, 287 (2015).
[6]V. Giannini, A. I. Fernández-Domínguez, S. C. Heck, and S. A. Maier, "Plasmonic nanoantennas: Fundamentals and their use in controlling the radiative properties of nanoemitters," Chem. Rev. **111**, 3888 (2011).
[7]S. J. Oldenburg, R. D. Averitt, S. L. Westcott, and N. J. Halas, "Nanoengineering of optical resonances," Chem. Phys. Lett. **288**, 243 (1998).
[8]X. Huang, S. Neretina, and M. A. El-Sayed, "Gold nanorods: From synthesis and properties to biological and biomedical applications," Adv. Mater. **21**, 4880 (2009).
[9]P. L. Stiles, J. A. Dieringer, N. C. Shah, and R. P. Van Duyne, "Surface-enhanced Raman spectroscopy," Annu. Rev. Anal. Chem. **1**, 601 (2008).
[10]M. Kauranen and A. V. Zayats, "Nonlinear plasmonics," Nat. Photonics **6**, 737 (2012).
[11]M. R. Shcherbakov, A. T. Le, N. Dubrovina, A. Lupu, and A. A. Fedyanin, "Plasmon ruler with gold nanorod dimers: Utilizing the second-order resonance," Opt. Lett. **40**, 1571 (2015).
[12]N. Meinzer, W. L. Barnes, and I. R. Hooper, "Plasmonic meta-atoms and metasurfaces," Nat. Photonics **8**, 889 (2014).
[13]P. Genevet, F. Capasso, F. Aieta, M. Khorasaninejad, and R. Devlin, "Recent advances in planar optics: From plasmonic to dielectric metasurfaces," Optica **4**, 139 (2017).
[14]S. A. Maier, M. L. Brongersma, P. G. Kik, S. Meltzer, A. A. G. Requicha, and H. A. Atwater, "Plasmonics: A route to nanoscale optical devices," Adv. Mater. **13**, 1501 (2001).
[15]D. K. Gramotnev and S. I. Bozhevolnyi, "Plasmonics beyond the diffraction limit," Nat. Photonics **4**, 83 (2010).
[16]N. Jiang, X. Zhuo, and J. Wang, "Active plasmonics: Principles, structures, and applications," Chem. Rev. **118**, 3054 (2018).
[17]V. V. Temnov, "Ultrafast acousto-magneto-plasmonics," Nat. Photonics **6**, 728 (2012).
[18]T. Srivastava, R. Das, and R. Jha, "Highly sensitive plasmonic temperature sensor based on photonic crystal surface plasmon waveguide," Plasmonics **8**, 515 (2013).
[19]A. E. Cetin, A. Mertiri, M. Huang, S. Erramilli, and H. Altug, "Thermal tuning of surface plasmon polaritons using liquid crystals," Adv. Opt. Mater. **1**, 915 (2013).
[20]J. Peng, H.-H. Jeong, Q. Lin, S. Cormier, H.-L. Liang, M. F. L. De Volder, S. Vignolini, and J. J. Baumberg, "Scalable electrochromic nanopixels using plasmonics," Sci. Adv. **5**, eaaw2205 (2019).
[21]J. Švanda, Y. Kalachyova, P. Slepička, V. Švorčík, and O. Lyutakov, "Smart component for switching of plasmon resonance by external electric field," ACS Appl. Mater. Interfaces **8**, 225 (2016).

[22]V. K. Belyaev, V. V. Rodionova, A. A. Grunin, M. Inoue, and A. A. Fedyanin, "Magnetic field sensor based on magnetoplasmonic crystal," Sci. Rep. **10**, 7133 (2020).
[23]V. V. Temnov, G. Armelles, U. Woggon, D. Guzatov, A. Cebollada, A. García-Martín, J.-M. Garcia-Martin, T. Thomay, A. Leitenstorfer, and R. Bratschitsch, "Active magneto-plasmonics in hybrid metal–ferromagnet structures," Nat. Photonics **4**, 107 (2010).
[24]M. Pohl, V. I. Belotelov, I. A. Akimov, S. Kasture, A. S. Vengurlekar, A. V. Gopal, A. K. Zvezdin, D. R. Yakovlev, and M. Bayer, "Plasmonic crystals for ultrafast nanophotonics: Optical switching of surface plasmon polaritons," Phys. Rev. B **85**, 081401 (2012).
[25]N. Rotenberg, M. Betz, and H. M. van Driel, "Ultrafast control of grating-assisted light coupling to surface plasmons," Opt. Lett. **33**, 2137 (2008).
[26]I. A. Novikov, M. A. Kiryanov, P. K. Nurgalieva, A. Y. Frolov, V. V. Popov, T. V. Dolgova, and A. A. Fedyanin, "Ultrafast magneto-optics in nickel magnetoplasmonic crystals," Nano Lett. **20**, 8615 (2020).
[27]G. Armelles, A. Cebollada, A. García-Martín, and M. U. González, "Magnetoplasmonics: Combining magnetic and plasmonic functionalities," Adv. Opt. Mater. **1**, 10 (2013).
[28]N. Maccaferri, "Coupling phenomena and collective effects in resonant meta-atoms supporting both plasmonic and (opto-)magnetic functionalities: An overview on properties and applications," J. Opt. Soc. Am. B **36**, E112 (2019).
[29]V. I. Safarov, V. A. Kosobukin, C. Hermann, G. Lampel, J. Peretti, and C. Marlière, "Magneto-optical effects enhanced by surface plasmons in metallic multilayer films," Phys. Rev. Lett. **73**, 3584 (1994).
[30]M. Rollinger, P. Thielen, E. Melander, E. Östman, V. Kapaklis, B. Obry, M. Cinchetti, A. García-Martín, M. Aeschlimann, and E. T. Papaioannou, "Light localization and magneto-optic enhancement in Ni antidot arrays," Nano Lett. **16**, 2432 (2016).
[31]J. Y. Chin, T. Steinle, T. Wehlus, D. Dregely, T. Weiss, V. I. Belotelov, B. Stritzker, and H. Giessen, "Nonreciprocal plasmonics enables giant enhancement of thin-film Faraday rotation," Nat. Commun. **4**, 1599 (2013).
[32]A. A. Grunin, A. G. Zhdanov, A. A. Ezhov, E. A. Ganshina, and A. A. Fedyanin, "Surface-plasmon-induced enhancement of magneto-optical Kerr effect in all-nickel subwavelength nanogratings," Appl. Phys. Lett. **97**, 261908 (2010).
[33]A. A. Grunin, N. A. Sapoletova, K. S. Napolskii, A. A. Eliseev, and A. A. Fedyanin, "Magnetoplasmonic nanostructures based on nickel inverse opal slabs," J. Appl. Phys. **111**, 07A948 (2012).
[34]A. V. Chetvertukhin, A. A. Grunin, A. V. Baryshev, T. V. Dolgova, H. Uchida, M. Inoue, and A. A. Fedyanin, "Magneto-optical Kerr effect enhancement at the wood's anomaly in magnetoplasmonic crystals," J. Magn. Magn. Mater. **324**, 3516 (2012).
[35]N. Kostylev, I. S. Maksymov, A. O. Adeyeye, S. Samarin, M. Kostylev, and J. F. Williams, "Plasmon-assisted high reflectivity and strong magneto-optical Kerr effect in permalloy gratings," Appl. Phys. Lett. **102**, 121907 (2013).
[36]M. G. Barsukova, A. S. Shorokhov, A. I. Musorin, D. N. Neshev, Y. S. Kivshar, and A. A. Fedyanin, "Magneto-optical response enhanced by Mie resonances in nanoantennas," ACS Photonics **4**, 2390 (2017).
[37]N. Maccaferri, X. Inchausti, A. García-Martín, J. C. Cuevas, D. Tripathy, A. O. Adeyeye, and P. Vavassori, "Resonant enhancement of magneto-optical activity induced by surface plasmon polariton modes coupling in 2D magnetoplasmonic crystals," ACS Photonics **2**, 1769 (2015).
[38]I. Zubritskaya, K. Lodewijks, N. Maccaferri, A. Mekonnen, R. K. Dumas, J. Åkerman, P. Vavassori, and A. Dmitriev, "Active magnetoplasmonic ruler," Nano Lett. **15**, 3204 (2015).
[39]N. Maccaferri, K. E. Gregorczyk, T. V. A. G. de Oliveira, M. Kataja, S. van Dijken, Z. Pirzadeh, A. Dmitriev, J. Åkerman, M. Knez, and P. Vavassori, "Ultrasensitive and label-free molecular-level detection enabled by light phase control in magnetoplasmonic nanoantennas," Nat. Commun. **6**, 6150 (2015).
[40]V. Bonanni, S. Bonetti, T. Pakizeh, Z. Pirzadeh, J. Chen, J. Nogués, P. Vavassori, R. Hillenbrand, J. Åkerman, and A. Dmitriev, "Designer magnetoplasmonics with nickel nanoferromagnets," Nano Lett. **11**, 5333 (2011).
[41]A. A. Grunin, I. R. Mukha, A. V. Chetvertukhin, and A. A. Fedyanin, "Refractive index sensor based on magnetoplasmonic crystals," J. Magn. Magn. Mater. **415**, 72 (2016).
[42]V. I. Belotelov, I. A. Akimov, M. Pohl, V. A. Kotov, S. Kasture, A. S. Vengurlekar, A. V. Gopal, D. R. Yakovlev, A. K. Zvezdin, and M. Bayer, "Enhanced magneto-optical effects in magnetoplasmonic crystals," Nat. Nanotechnol. **6**, 370 (2011).
[43]G. A. Wurtz, W. Hendren, R. Pollard, R. Atkinson, L. L. Guyader, A. Kirilyuk, T. Rasing, I. I. Smolyaninov, and A. V. Zayats, "Controlling optical transmission through magneto-plasmonic crystals with an external magnetic field," New J. Phys. **10**, 105012 (2008).
[44]D. Martín-Becerra, J. B. González-Díaz, V. V. Temnov, A. Cebollada, G. Armelles, T. Thomay, A. Leitenstorfer, R. Bratschitsch, A. García-Martín, and M. U. González, "Enhancement of the magnetic modulation of surface plasmon polaritons in Au/Co/Au films," Appl. Phys. Lett. **97**, 183114 (2010).
[45]C. Clavero, K. Yang, J. R. Skuza, and R. A. Lukaszew, "Magnetic field modulation of intense surface plasmon polaritons," Opt. Express **18**, 7743 (2010).
[46]C. Clavero, K. Yang, J. R. Skuza, and R. A. Lukaszew, "Magnetic-field modulation of surface plasmon polaritons on gratings," Opt. Lett. **35**, 1557 (2010).
[47]A. Y. Frolov, M. R. Shcherbakov, and A. A. Fedyanin, "Dark mode enhancing magneto-optical Kerr effect in multilayer magnetoplasmonic crystals," Phys. Rev. B **101**, 045409 (2020).
[48]A. V. Chetvertukhin, A. I. Musorin, T. V. Dolgova, H. Uchida, M. Inoue, and A. A. Fedyanin, "Transverse magneto-optical Kerr effect in 2D gold–garnet nanogratings," J. Magn. Magn. Mater. **383**, 110 (2015).
[49]A. I. Musorin, A. V. Chetvertukhin, T. V. Dolgova, H. Uchida, M. Inoue, B. S. Luk'yanchuk, and A. A. Fedyanin, "Tunable multimodal magnetoplasmonic metasurfaces," Appl. Phys. Lett. **115**, 151102 (2019).
[50]M. Kataja, T. K. Hakala, A. Julku, M. J. Huttunen, S. van Dijken, and P. Törmä, "Surface lattice resonances and magneto-optical response in magnetic nanoparticle arrays," Nat. Commun. **6**, 7072 (2015).
[51]N. Maccaferri, L. Bergamini, M. Pancaldi, M. K. Schmidt, M. Kataja, S. v. Dijken, N. Zabala, J. Aizpurua, and P. Vavassori, "Anisotropic nanoantenna-based magnetoplasmonic crystals for highly enhanced and tunable magneto-optical activity," Nano Lett. **16**, 2533 (2016).
[52]R. M. Rowan-Robinson, E. Melander, I.-A. Chioar, B. Caballero, A. García-Martín, E. T. Papaioannou, and V. Kapaklis, "Thickness dependent enhancement of the polar Kerr rotation in Co magnetoplasmonic nanostructures," AIP Adv. **9**, 025317 (2019).
[53]Z. Tang, R. Zhu, L. Chen, C. Zhang, Z. Zong, S. Tang, and Y. Du, "Tuning the magneto-optical Kerr effect by the nanograting cross section," Opt. Lett. **44**, 1666 (2019).
[54]L. Halagačka, M. Vanwolleghem, F. Vaurette, J. Ben Youssef, K. Postava, J. Pištora, and B. Dagens, "Magnetoplasmonic nanograting geometry enables optical nonreciprocity sign control," Opt. Express **26**, 31554 (2018).
[55]A. López-Ortega, M. Zapata-Herrera, N. Maccaferri, M. Pancaldi, M. Garcia, A. Chuvilin, and P. Vavassori, "Enhanced magnetic modulation of light polarization exploiting hybridization with multipolar dark plasmons in magnetoplasmonic nanocavities," Light Sci. Appl. **9**, 49 (2020).
[56]D. Floess, M. Hentschel, T. Weiss, H. Habermeier, J. Jiao, S. Tikhodeev, and H. Giessen, "Plasmonic analog of electromagnetically induced absorption leads to giant thin film Faraday rotation of 14°," Phys. Rev. X **7**, 021048 (2017).
[57]S. Collin, "Nanostructure arrays in free-space: Optical properties and applications," Rep. Prog. Phys. **77**, 126402 (2014).
[58]R. A. Watts, A. P. Hibbins, and J. R. Sambles, "The influence of grating profile on surface plasmon polariton resonances recorded in different diffracted orders," J. Mod. Opt. **46**, 2157 (1999).
[59]S. T. Koev, A. Agrawal, H. J. Lezec, and V. A. Aksyuk, "An efficient large-area grating coupler for surface plasmon polaritons," Plasmonics **7**, 269 (2012).
[60]W. L. Barnes, A. Dereux, and T. W. Ebbesen, "Surface plasmon subwavelength optics," Nature **424**, 824 (2003).
[61]E. Loewen and E. Popov, *Diffraction Gratings and Applications* (Marcel Dekker, 1997).
[62]M. B. Sobnack, W. C. Tan, N. P. Wanstall, T. W. Preist, and J. R. Sambles, "Stationary surface plasmons on a zero-order metal grating," Phys. Rev. Lett. **80**, 5667 (1998).

[63]Z. Chen, I. R. Hooper, and J. R. Sambles, "Low dispersion surface plasmon-polaritons on deep silver gratings," J. Mod. Opt. **53**, 1569 (2006).
[64]V. I. Belotelov, D. A. Bykov, L. L. Doskolovich, A. N. Kalish, and A. K. Zvezdin, "Extraordinary transmission and giant magneto-optical transverse Kerr effect in plasmonic nanostructured films," J. Opt. Soc. Am. B **26**, 1594 (2009).
[65]H. Raether, "Surface plasmons on smooth surfaces," in *Surface Plasmons on Smooth and Rough Surfaces and on Gratings* (Springer, 1988).
[66]S. Maier, *Plasmonics: Fundamentals and Applications* (Springer, 2007).
[67]G. Dayal, A. Solanki, X. Y. Chin, T. C. Sum, C. Soci, and R. Singh, "High-Q plasmonic infrared absorber for sensing of molecular resonances in hybrid lead halide perovskites," J. Appl. Phys. **122**, 073101 (2017).
[68]T. J. Seok, A. Jamshidi, M. Kim, S. Dhuey, A. Lakhani, H. Choo, P. J. Schuck, S. Cabrini, A. M. Schwartzberg, J. Bokor, E. Yablonovitch, and M. C. Wu, "Radiation engineering of optical antennas for maximum field enhancement," Nano Lett. **11**, 2606 (2011).
[69]K. Koshelev, Y. Tang, K. Li, D.-Y. Choi, G. Li, and Y. Kivshar, "Nonlinear metasurfaces governed by bound states in the continuum," ACS Photonics **6**, 1639 (2019).
[70]P. Johnson and R. Christy, "Optical constants of transition metals: Ti, V, Cr, Mn, Fe, Co, Ni, and Pd," Phys. Rev. B **9**, 5056 (1974).
[71]G. S. Krinchik and V. A. Artem'ev, "Magneto-optical properties of Ni, Co, and Fe in the ultraviolet visible, and infrared parts of spectrum," Sov. Phys. JETP **26**, 1080–1085 (1968).
[72]M. Pohl, L. E. Kreilkamp, V. I. Belotelov, I. A. Akimov, A. N. Kalish, N. E. Khokhlov, V. J. Yallapragada, A. V. Gopal, M. Nur-E-Alam, M. Vasiliev, D. R. Yakovlev, K. Alameh, A. K. Zvezdin, and M. Bayer, "Tuning of the transverse magneto-optical Kerr effect in magneto-plasmonic crystals," New J. Phys. **15**, 075024 (2013).
[73]D. O. Ignatyeva, D. Karki, A. A. Voronov, M. A. Kozhaev, D. M. Krichevsky, A. I. Chernov, M. Levy, and V. I. Belotelov, "All-dielectric magnetic metasurface for advanced light control in dual polarizations combined with high-Q resonances," Nat. Commun. **11**, 5487 (2020).